JOURNAL OF MATERIALS SCIENCE 26 (1991) 4241–4249

Strengthening mechanisms in whisker-reinforced aluminium composites

C. VOITURIEZ, I. W. HALL
Materials Science Program, Spencer Laboratory, University of Delaware, Newark, DE 19716, USA

Silicon carbide whisker reinforced aluminium alloys were mechanically tested in the as-cast and heat treated conditions; the microstructures were examined by transmission electron microscopy. The mechanical properties were strongly dependent upon the nature of the matrix alloying elements, the heat treatment conditions and the processing routes. Al–Cu and Al 6061 reinforced alloys were very responsive to heat treatment while Al–Mg and Al–Si reinforced alloys were not. The microstructures and mechanical properties were analysed in an attempt to determine the operative strengthening mechanisms and deformation processes. Three distinct types of matrix microstructure were observed, distinguished by the presence or absence of subgrains and/or precipitates. Using these observations, the composite properties could be quite well modelled using dislocation theories, indicating that the matrix microstructure dominates the mechanical properties.

1. Introduction

Silicon carbide whisker-reinforced aluminium metal matrix composites have been under development for several years now and considerable effort has been directed towards modelling the strengthening mechanisms which operate. The basic strengthening mechanisms which are believed to occur are load transfer (from the matrix to the whiskers), precipitation hardening (in age-hardenable alloys), dispersion hardening (due to the whiskers), high dislocation density (generated at the interface), and residual elastic stresses (generated at the interface). Because a good overview of the different strengthening theories in short fibre-reinforced SiC/Al was recently given by Papazian and Adler [1], they will only be briefly summarized here.

A modified version of the basic discontinuous composite strengthening model, based on load transfer by shear (shear lag model), was proposed by Nardone and Prewo [2, 3] in which a term was incorporated to account for tensile stress transfer at fibre ends when aspect ratios are low (modified shear lag model). Their calculations were related to experimental observations made on a P/M $20V_f$% SiC/6061 composite and gave good predictions of the yield strength. Taya and Arsenault [4] also developed an Eshelby-type model to predict the yield strength. However, these models generally predict yield strengths which are less than the experimental values. They assume that the matrix properties are unchanged by the addition of SiC whiskers and ignore the higher dislocation densities and work hardening rates observed in the composite. They are, therefore, limited when describing plastic behaviour. An alternative to this approach has been proposed by Levy and Papazian [5], who developed finite element models, using the observed mechanical properties of the matrix and the ceramic phase and based on three-dimensional arrays of aligned undirectional cylinders. They were able to account for nonlinear behaviour and to describe the initiation and propagation of plastic deformation between the fibres.

These models are based on a continuum approach and assume that load transfer occurs between the fibres and the matrix. Others have used a micromechanical approach which uses dislocation theories to predict the strength [6–8], where the mechanical behaviour of the composite is described on the basis of dispersoid rather than composite strengthening. The objective of the micromechanical approach is to determine the contribution of the microstructure to the yield strength. The main microstructural features contributing to the flow stress are the internal stresses, the grains and subgrains, the solute atoms through solute hardening, the whiskers and the precipitates through dispersion and precipitation hardening, respectively.

The role of the thermal residual stresses in the strengthening of the SiC_w/Al composites has also been investigated [9–11]. High dislocation densities have been observed in SiC_w/Al composites to develop as a result of the relief of the thermal stresses arising because of the difference in coefficients of thermal expansion between the matrix and the whiskers [12, 13]. Models have been developed to determine the increase in strength due to these dislocations. Several investigations reviewed and compared the predictions of shear lag and dislocation models but without being able to reach a consensus [3, 4]. It is still unclear whether load transfer or matrix microstructure is the main source of strengthening. However, in squeeze-cast

0022–2461/91 $03.00 + .12

composites, where the reinforcement phase is randomly oriented, the matrix microstructure is believed to have a strong influence on the strength.

The focus of the present work was, therefore, to characterize the strengthening mechanisms and deformation processes occurring in random short-fibre MMCs, and to examine the effects of changes in matrix microstructure on the overall composite properties. The effects of alloying elements, heat treatments and processing routes on the tensile properties of various SiC_w/Al composites were investigated, with a particular interest in the elastic/plastic transition. The first stage of the work consisted of testing the reinforced and unreinforced alloys. Scanning electron microscopy (SEM) was used to examine the fracture surfaces and transmission electron microscopy (TEM) was used to determine the deformation modes occurring in the materials and to examine the microstructure of the composites prior to deformation. The TEM observations were mainly aimed at determining the microstructural factors influencing the yield strength and contributing to the composite strengthening. Micromechanical models were then considered and their predictions will be compared to the experimental data obtained in this study. In order to clarify the role of the thermally induced dislocations on the ageing process and on the strengthening mechanisms of the SiC_w/Al composites, an ageing study of the Al–4%Cu composite was performed as well as some refrigeration experiments.

2. Experimental procedure

In order to separate the effects of different alloying elements upon the strength of the composites, the following three simple binary alloy matrices were used; Al–5Si, a common aluminium casting alloy; Al–2Mg, a system used where improved wetting of the ceramic phase is required; Al–4Cu, selected for its age-hardening potential. Finally Al 6061, a commercial alloy with a nominal composition of Al–0.6Si–1Mg–0.28Cu–0.2Cr, was used to study the effect of more complex alloy chemistry. The reinforcement was 20 V_f% SiC in whisker form. Before processing the whisker diameter and lengths were about 0.5 μm and 5–50 μm, respectively. The specimens were manufactured via a squeeze-casting technique.

The composites were tensile tested in the as-fabricated (F) and heat-treated (T6) condition. The Al 6061 composites were solution treated at 530 °C for 3 h, water quenched and aged at 170 °C for 8 h. The binary alloy composites were solution treated at 525 °C for 8 h, quenched and aged at 190 °C for 24 h. Corresponding unreinforced binary alloys were also tested in order to determine the strengthening effects of the whiskers on the different alloys. They were prepared using the same processing routes and heat treatments as for the composites. The only difference was that the grain size of the unreinforced alloys was greater than that of the reinforced alloys.

A second set of Al–4%Cu composites containing $\sim 15 V_f$% of SiC_w was manufactured for additional ageing and refrigeration experiments. Some of these were solution treated and aged for different times at 190 °C and age-hardening curves constructed from hardness test data. Tensile specimens were then prepared and tested in the underaged, peak aged and overaged conditions. Also, because residual stresses are known to exert an influence upon composite properties, other samples were subjected to refrigeration experiments in order to maximize the ΔT values. Refrigeration in liquid N_2 for 10 h was carried out both after ageing and between the quenching and ageing steps.

Tensile tests were conducted at room temperature on an 1125 Instron testing machine. The reinforced samples had a cylindrical reduced gauge length of 17 mm, a cross-sectional area of 28.3 mm^2 and were tested at a strain rate of $10^{-4}\ s^{-1}$. The unreinforced alloy tensile specimens were rectangular in cross-section with a gauge length of 25.4 mm and a cross-sectional area of 20 mm^2; they were tested at a strain rate of $2 \times 10^{-5}\ s^{-1}$. Each reported data point represents the average (and standard deviation) of six tensile tests.

Polished and etched longitudinal and transverse sections of all composites were examined by optical microscopy and SEM in order to characterize the as-fabricated microstructure. Fracture surfaces were also examined by SEM. Transmission electron microscopy samples were prepared by standard ion-milling techniques both from deformed (below the fracture surface) and undeformed composites to determine the deformation modes operating in the materials.

3. Results

3.1. Tensile tests

The results of all the tensile tests are presented in Table I. Young's modulus, E, yield strength, YS, and

TABLE I Results of the tensile tests

Materials	E_c (GPa)	E_m (GPa)	YS_c (MPa)	YS_m (MPa)	UTS_c (MPa)	ε_{fc}	ε_{fm}
6061–T6	107.4(±1)	–	375(±13)	–	550(±19)	2.23(±0.1)	–
Al–4%Cu–F	107.8(±1)	70(±7)	182(±13)	70(±7)	480(±17)	4.15(±0.3)	–
Al–4%Cu–T6	105.8(±14)	74(±4)	308(±4)	144(±0)	577(±7)	3.2(±0.3)	–
Al–5%Si–F	105(±2)	88(±1)	155(±8)	62(±1)	405(±6)	3.13(±0.3)	–
Al–5%Si–T6	108.7(±7)	60(±10)	166(±11)	52(±1)	440(±6)	2.84(±0.1)	8.6(±0.4)
Al–2%Mg–F	124(±2)	86(±3)	184.5(±15)	67(±2)	480(±16)	3.18(±0.1)	10.2(±0.4)
Al–2%Mg–T6	91(±2)	69(±10)	209(±13)	95(±4)	447(±18)	3.74(±0.4)	–

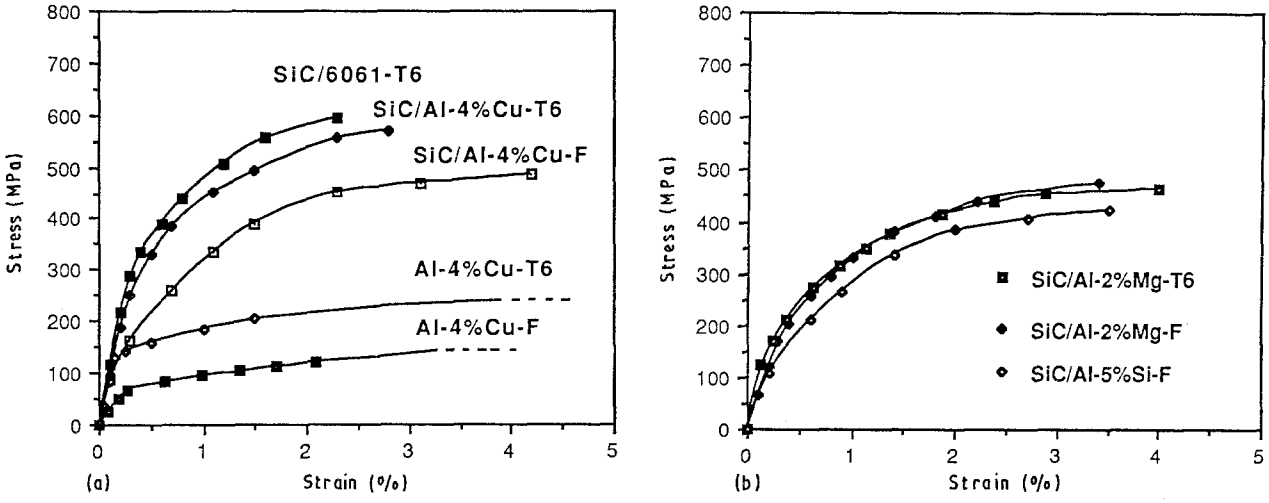

Figure 1 Representative stress-strain curves for (a) age hardenable alloys and composites, and (b) non-age hardenable composites.

ultimate tensile strength, UTS, were greatly increased by the introduction of whiskers to any of the matrices. On the other hand, the strains to failure, ε_f, dropped considerably from about 10% to about 3% (subscripts c and m refer to composite and matrix, respectively).

Two general categories of stress–strain curves can be distinguished and are illustrated in Fig. 1a and b, namely, the age-hardenable (Al 6061, Al–4%Cu) and non-age-hardenable materials (Al–5%Si, Al–2%Mg). The age-hardened materials (composites and alloys) exhibit long elastic regions, resulting in higher yield and ultimate strengths. However, Table I shows that the increase in YS due to heat treatment is higher for the composites than for the unreinforced alloys: ΔYS (T6 − F) = 74 MPa for Al–4%Cu and 126 MPa for SiC_w/Al–4%Cu, showing that the composite reacts to heat treatment differently. In Al–5%Si and Al–2%Mg composites, the introduction of whiskers in the matrix gave an increase in yield strength of about 100 MPa and this was almost unaffected by the heat treatment. However, the increase in YS of the T6 Al–4%Cu alloy due to the reinforcement phase is higher than that of the F Al–4%Cu alloy: ΔYS (20%V_f–0%V_f) = 112 MPa for the F material and 164 MPa for the T6 material. This again implies that the strengthening effect of the whiskers is greater in age-hardenable materials. This point will be considered further in the discussion below. Table I also shows that, of the non-heat-treatable composites, the Al–2%Mg matrix composites have the higher yield strengths, probably due to significant solid solution strengthening.

The ageing experiments showed that peak hardness was achieved in the unreinforced and reinforced Al–4% Cu samples after ~20 h and 8 h, respectively. However, the increase in hardness due to ageing was much smaller for the composite than for the matrix. Tensile tests were carried out on peak aged, underaged and overaged reinforced specimens (t = 8 h, 30 min, 100 h, respectively). These specimens exhibited very low ductilities ($\varepsilon_f \approx 1\%$), attributed to their being prepared from a different set of preforms which, judging from the appearance of the fracture surfaces, contained rather a high concentration of large SiC debris particles. The results of the tests are shown in Table II. The increase in yield strength between the peak aged and underaged composites, ΔYS (peak aged − underaged) = 70 MPa. But, as expected from the hardening curves, there was little difference between the peak aged and overaged conditions.

TABLE II Tensile test results for underaged, peak aged and overaged $SiC_w(15V_f\%)$/Al–Cu composites

Ageing condition	E(GPa)	YS_c(MPa)	YS_m(MPa)
Underaged	93(±2)	174(±5)	70(±7)
Peak aged	96(±5)	250(±7)	144(±0)
Overaged	96(±20)	250(±12)	–

Results of tensile tests on the refrigerated samples are shown in Table III and comparison with the data of Table II shows that significant increases in strength occur. For underaged samples the increase is ~43 MPa and for peak aged or overaged samples the increase is ~35 MPa. Also it is seen that the timing of the refrigeration treatment, i.e. before or after the ageing step, is of no consequence for the mechanical properties.

3.2. Fractography

In most of the specimens, macrocracks appear to diverge from one or several types of initiation site, Fig. 2a. These sites are generally internal defects such as silicon carbide debris, clusters of SiC whiskers, porosity, intermetallic inclusions or areas of high Ca content occurring during processing. Others are surface defects which may have occurred during machining or handling and all of these defects are believed to contribute to the low ductility of these composites. On the microscopic scale, the fracture surfaces are characterized by the presence of dimples of various depths and diameters, indicating ductile fracture of the matrix. Whisker ends appear at the centre or at the edges of the dimples, Fig. 2b. Little pull-out is observed and the few pulled out whiskers are coated with a thin

TABLE III Results of the tensile tests of the refrigerated composites

Heat treatment	E (GPa)	YS (MPa)	YS (MPa) (no refrigeration)
Solution treated–quenched–refrigerated–aged (8 h at 190 °C)	95.7(±1)	287(±30)	250(±7)
Solution treated–quenched–aged (8 h at 190 °C)–refrigerated	95.5(±1)	283(±3)	250(±7)
Solution treated–quenched–aged (30 min at 190 °C)–refrigerated	94.5(±1)	217(±3)	174(±5)

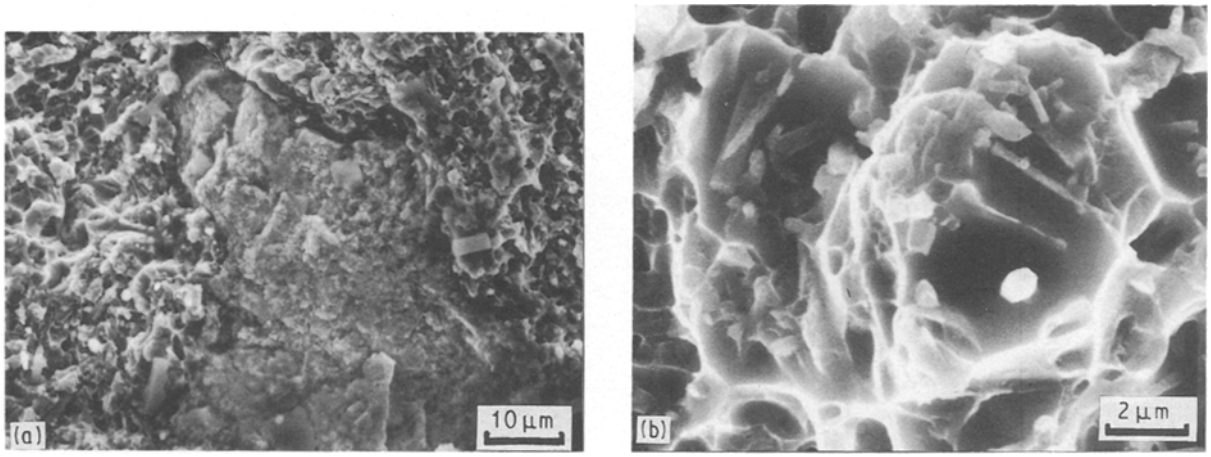

Figure 2 (a) Fracture initiation at the edge (lower right) of tensile specimen. A large (>60 μm,) Fe-rich inclusion occupies most of the micrograph. (b) Fracture surface of SiC_w/Al–Cu composite showing dimples nucleated by whiskers.

layer of matrix showing that there is a good bond between the SiC and the matrix. The tensile ductilities of the main group of specimens appeared to be essentially independent of the matrix microstructure and the fracture surfaces have the same macroscopic and microscopic appearance.

3.3. Metallography

SEM of polished and etched sections showed that there was no preferred whisker orientation and ageing did not have any effect noticeable at this level of magnification. The Cu-containing specimens (Al–4% Cu–T6 and F) showed regions where the whiskers were closely packed together along with a strongly wetting Cu-rich phase, Fig. 3a. Microporosity, associated with individual whiskers, Fig. 3b, was observed in most specimens except those containing Si. Many large pores up to ~15 μm diameter were observed in 6061 samples, Fig. 3b, and to a lesser extent in the Al–Cu samples.

Samples from the strained and unstrained materials were then examined by TEM. Considering first the unstrained material, characteristic second-phase particles were observed at the whisker/matrix interface in the Cu-containing composites, Fig. 4a. They were identified by energy dispersive X-ray analysis and X-ray diffraction as either $CuAl_2$ precipitates or phases containing iron (Fe_3SiAl_{12} or Cu_2FeAl_7) which wet the surface of the whisker. Disc-shaped θ′ precipitates, ~100 nm diameter, were observed throughout the matrix of as-fabricated composites. After heat treatment, these precipitates increased in number and in size to $\sim 3\text{–}4 \times 10^2$ nm, Fig. 4b.

In the as-fabricated Al–5%Si specimen no precipitates were found in the matrix but fine rod-shaped precipitates did appear in the T6 condition. They mainly contained silicon and appeared in areas of high dislocation density. Because a small quantity of iron is present in the matrix, these particles were probably β(FeSi) compounds. They could be responsible for the slight increase in yield strength which is noted when comparing the F and T6 composites. Interfacial precipitates were not generally observed.

The Al–Mg matrix composites are also non-heat treatable and no fine scale matrix precipitation occurred in these samples. Very fine precipitates were, however, frequently observed at the whisker/matrix interface and microdiffraction showed that both Mg_2Si and MgO particles were present, Fig. 5.

In the Al6061 composites relatively large numbers of Mg_2Si precipitates formed in the matrix, Fig. 6a, as well as the interface, Fig. 6b, and they formed a discontinuous layer in some cases.

In addition to the differences in precipitation phenomena between the various specimens noted above, there were also differences in the dislocation densities and substructures. In all the samples a large number of dislocations had been generated adjacent to the whiskers, particularly at the ends, due to the difference in expansion coefficients of the two components. In the Al–Cu and Al–Mg and Al6061 composites the dislocations remained in a random distribution, Fig. 7a, associated both with the whiskers and, when present, the precipitates. However, a very clear difference was that the Al–Si matrix composites contained a well-defined subgrain network instead of a random dislocation array, Fig. 7b.

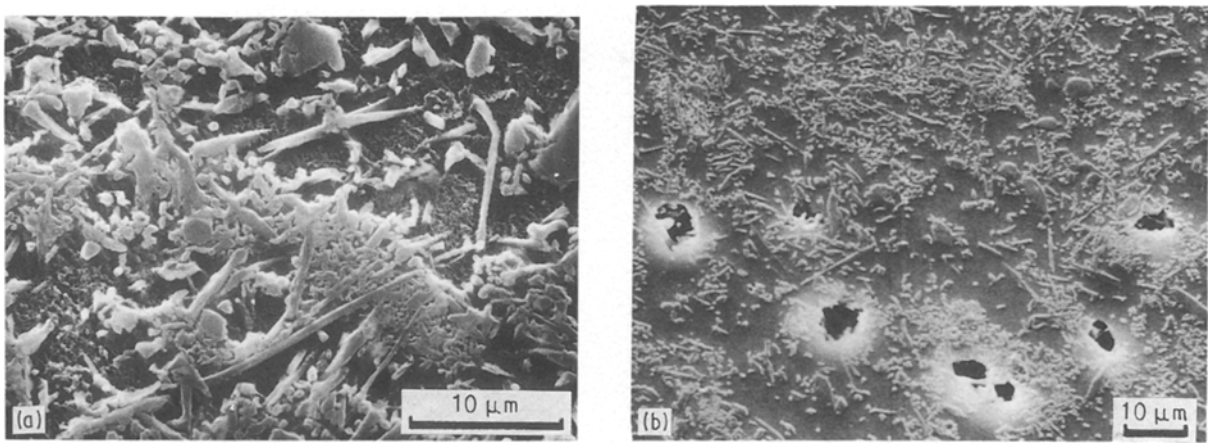

Figure 3 (a) Polished and lightly etched section of SiC_w/Al–Cu composite showing whiskers and strongly wetting $CuAl_2$. (b) Microporosity in SiC_w/Al 6061 composite.

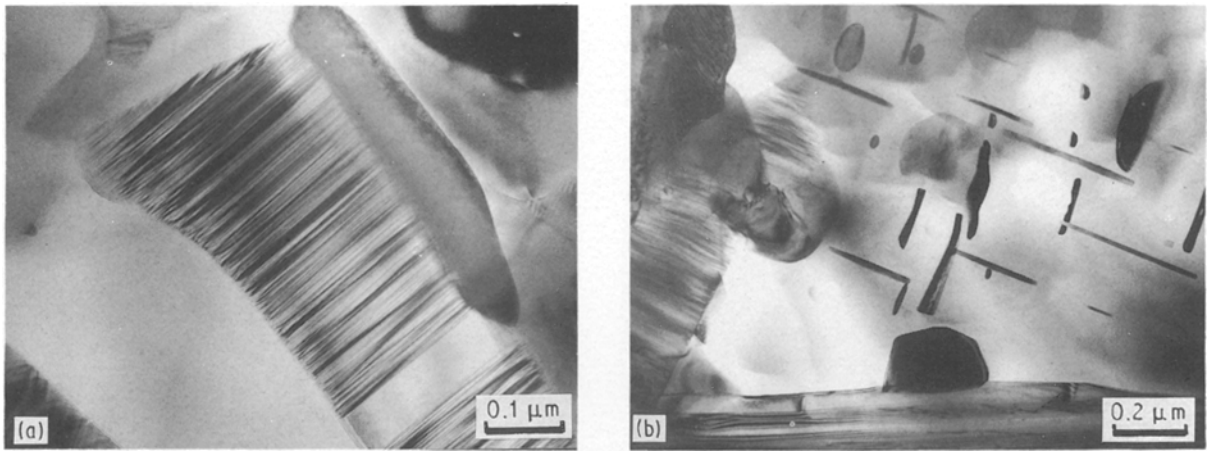

Figure 4 (a) $CuAl_2$ particle at whisker–matrix interface in as-cast SiC_w/Al–Cu composite. (b) θ′ precipitates in matrix and $CuAl_2$ at interface in aged SiC_w/Al–Cu composite.

In foils taken from fractured specimens it was seen that the dislocation sub-structures described previously were considerably modified by deformation, principally by the generation of subgrains in all the binary alloy composites in both the T6 and F conditions. The subgrains were generally of the same size as the inter-whisker spacing, i.e. 0.5–1 μm, as shown for an Al–2Mg specimen in Fig. 8. The 6061 composites did not exhibit a subgrain structure in either the undeformed or the deformed condition.

In the deformed composites with high ultimate strengths (6061 and Al–Cu heat-treated composites), cracked whiskers appeared quite often, Fig. 9a. In the Al–Mg composites, decohesion seemed to occur before whisker cracking, Fig. 9b. In contrast, the Al–Si specimens exhibited neither decohesion nor whisker cracking. These observations show that the extent of plastic flow of the matrix and its localization depend on the alloying elements, which results in different deformation modes.

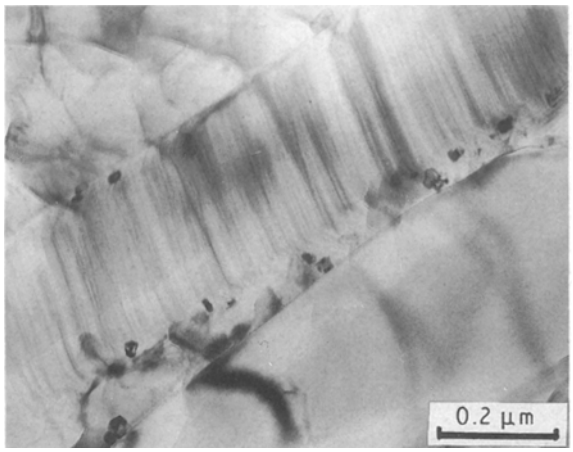

Figure 5 Fine-scale (~20–40 nm) grains of MgO at an interface in SiC_w/Al–2Mg composite.

4. Discussion

The results described above show that the microstructure of SiC_w/Al MMCs can be substantially modified due to matrix alloying effects and heat treatment and that the mechanical properties are correspondingly affected. Some of these effects are directly related to the dislocation arrangements and some depend upon the precipitation phenomena.

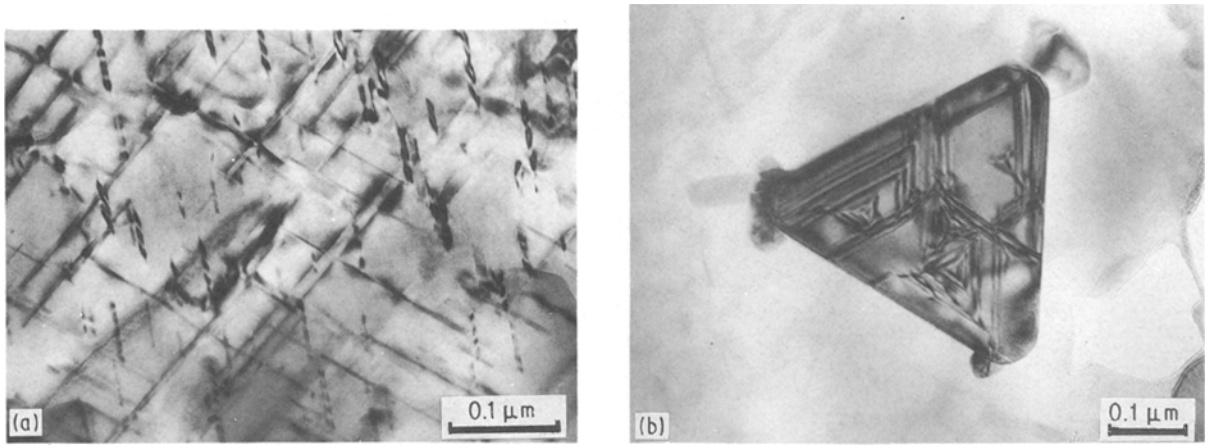

Figure 6 (a) Matrix precipitates of Mg_2Si in SiC_w/Al 6061 composite. (b) Mg_2Si precipitates at interface in SiC_w/Al 6061 composite.

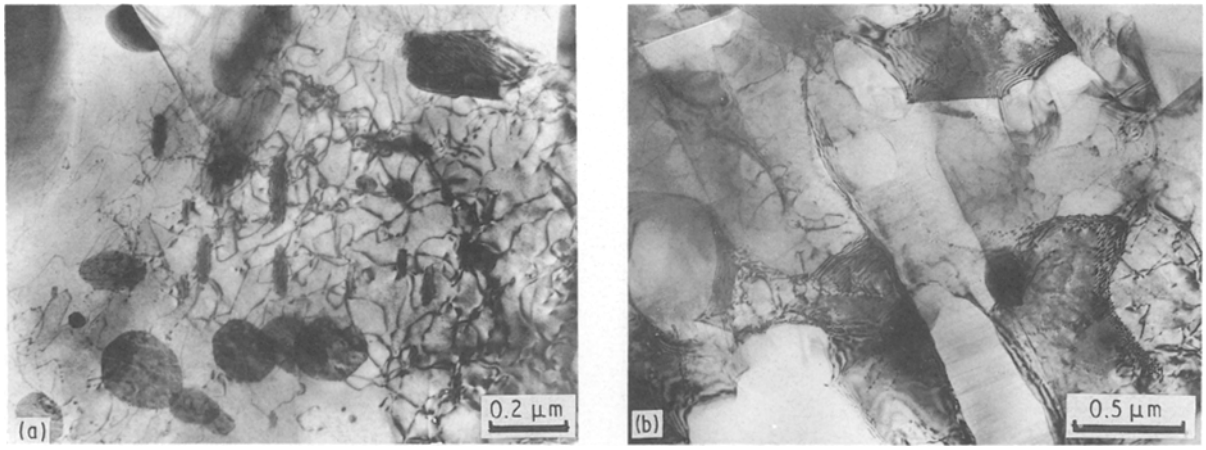

Figure 7 (a) Random dislocation tangle in as-cast SiC_w/Al–Cu composite. (b) Dislocations arranged in well-defined subgrains in as-cast SiC_w/Al–Si composite.

Because the coefficient of thermal expansion of the matrix is significantly greater than that of the reinforcement phase, the matrix is under a residual tensile stress and the reinforcement is left under a residual compressive stress upon cooling from the production temperature. The matrix tensile stresses are partially relieved by the generation of dislocations at the whisker interface. In the T6 materials additional dislocations are generated during quenching from the solution treatment temperature to room temperature ($\Delta T = 500\,^{\circ}C$). Such increases in dislocation density around the whiskers have been well documented in the literature. Vogelsang *et al.* [13] reported *in situ* experiments, conducted in a high-voltage electron microscope, where SiC_w/Al composites were cooled from different annealing temperatures. They clearly showed that the dislocation density can be greatly increased when the composite is cooled by $\Delta T = 500\,^{\circ}C$ and dislocation densities $> 10^{13}\,m^{-2}$ were measured. Several authors have developed models to predict the increase in yield strength as a result of the increased dislocation density but it is unlikely that the strengthening effects of the whiskers can be completely accounted for in this manner.

Figure 8 Characteristic subgrain structure in deformed SiC_w/Al–Mg composite.

In the present work, a substantial increase in yield strength due to thermal treatment is observed only in the age hardenable materials. The reason for there being only a modest (10–20 MPa) yield strength increase in the non-heat-treatable composites, even though they have been subjected to the same quenching (and ageing) treatments, is that the observed

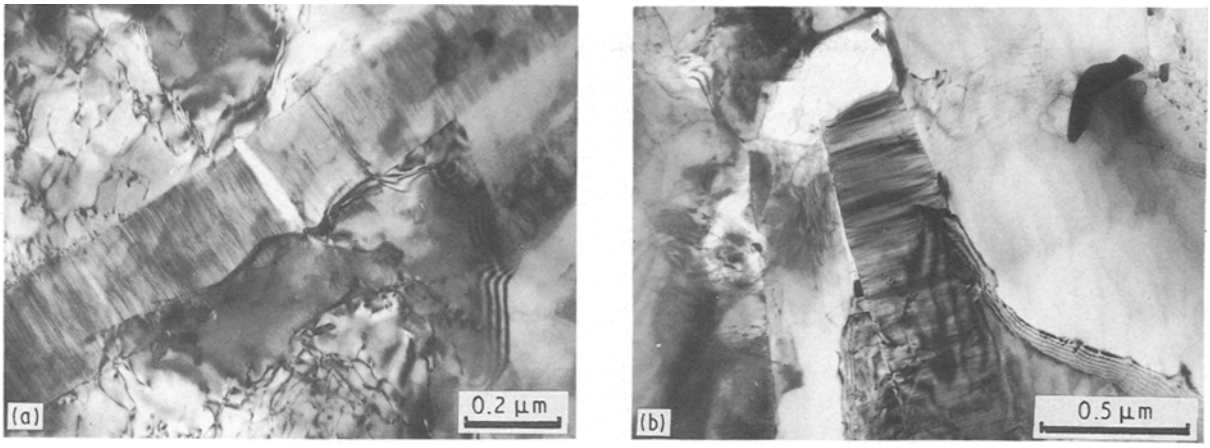

Figure 9 (a) Cracked whisker in deformed SiC_w/Al 6061 composite. (b) Decohesion at whisker/matrix interface in deformed SiC_w/Al–Mg composite.

dislocation structures in the F and T6 heat-treated composites are very similar. In F materials, dislocations are introduced on cooling from the manufacturing temperature while in T6 materials rather more are introduced and retained from the quenching step. In Al–Si composites, because of the low matrix yield strength, dislocations can even rearrange to the extent of forming subgrain boundaries.

On the other hand, in the case of heat-treatable composites, strong precipitate/dislocation interactions can occur and these depend on the heat-treatment condition. Dislocations generated at the whisker interface during quenching accelerate the precipitation process and the increase in yield strength which follows is enhanced by the punching out of dislocations by the precipitates. When precipitates are present in the matrix the mean free path of the dislocations is short, they are prevented from moving and often link the interface of the whisker to a particle close to it or two particles together, as shown in Fig. 7a. In this case (age-hardenable composites), the strengthening will depend on the size and distribution of the age-hardening particles and on their interactions with the dislocations present in the matrix of the composite. The importance of the matrix precipitates in increasing the strength has also been demonstrated by Papazian and Adler [1].

In this section the micromechanical approach, which has been well documented by Humphreys [8], will be used to model the strength properties. Three distinct types of matrix microstructure have been observed in the unstrained composites, namely, matrix + subgrains, matrix + precipitates + dislocations, and, finally, matrix + dislocations (no precipitates). The following model, therefore, uses dislocation theories to calculate the yield strength based upon the above observations of the microstructure. Yield will occur when stresses rise sufficiently to allow dislocation motion in the matrix. In the matrix, there are various barriers to dislocation motion such as grain and subgrain boundaries, whiskers, precipitates and internal stresses. Their respective contributions to the yield strength will be calculated below.

Grain and subgrain strengthening, σ_g, have been evaluated [8] and were found to be significant when considering grain sizes varying from 1–10 μm. The contribution to the yield strength due to grain size, d, is given by the well-known equation

$$\sigma_g = k_y d^{-1/2} \quad (1)$$

where the constant, k_y, is around 0.1 MPa $m^{1/2}$ for grains and 0.05 MPa $m^{1/2}$ for subgrains [14, 15]. As noted earlier, the grain size of the matrix with the whiskers is usually smaller than the grain size of the unreinforced matrix alone, therefore, it contributes to the increase in strength in the composite. For a subgrain size of 1 μm, as found in the Al–Si composites, $\sigma_g = 50$ MPa.

The strengthening contribution of the whiskers can be modelled using a dispersion hardening mechanism associated with unrelaxed Orowan loops. The strength increase is given by

$$\sigma_d \sim 2\mu b/s \quad (2)$$

where μ is the shear modulus of the matrix, $\boldsymbol{b}$ is Burger's vector and s is the interparticle spacing. This term does not contribute significantly to the strength increase in the present case ($\sim$15 MPa) but in the case of very fine reinforcements and high-volume fractions its contribution will be greater. Another alternative for modelling the strengthening effects of the whiskers is to use the prismatic dislocation punching model and this will be discussed further below.

Precipitation hardening occurs in age-hardened composites and its contribution can be determined experimentally using Equation 3

$$\sigma_p = \sigma_{cy}(T6) - \sigma_{cy}(F) \quad (3)$$

where σ_{cy} is the composite yield strength, T6 and F denote the treatment condition. $\sigma_p = 130$ MPa for the Al–Cu composite.

Additionally, solute strengthening, σ_s, and internal stresses, σ_i, may contribute to the strengthening. All these factors will contribute to the yield strength and the processing and heat treatments selected for the fabrication of the composite will determine the importance of their relative contributions. It was shown

by Foreman and Makin [16] that the contribution of strong obstacles, such as precipitates and dispersoids, is best represented by $(\sigma_p^2 + \sigma_d^2)^{1/2}$ and that the contribution of weaker obstacles, such as solute atoms, grains and internal stresses, can be added linearly. Hence, the resulting yield stress [8] is given by

$$\sigma_{cy} = (\sigma_p^2 + \sigma_d^2)^{1/2} + \sigma_i + \sigma_g + \sigma_s \quad (4)$$

When no subgrains develop in the matrix and if internal stresses are ignored for squeeze-cast composites, $\sigma_i + \sigma_g + \sigma_s$ could be replaced by σ_{my} [6], the matrix yield strength prior to heat treatment (no precipitation hardening). Also, Lederich and Sastry [6] proposed that if no precipitates are present in the matrix, the composite yield strength can be approximated by

$$\sigma_{cy} = (\sigma_{my}^2 + \sigma_d^2)^{1/2} \quad (5a)$$

or

$$\sigma_{my} + \sigma_d \quad (5b)$$

when $\sigma_{my} \gg \sigma_d$ where σ_{my} is the yield strength of the matrix. A grain-strengthening term should be added if subgrains develop in the matrix of the composite. This approach is a semi-empirical method which requires a good knowledge of the microstructure (grain size, interparticle spacing, etc.) of the composite. The additivity of the contribution of all the micromechanisms of strengthening can only give an approximate idea of the total strength of the composite but it gives a better understanding of the strengthening mechanisms operating in Al MMCs. To predict the strength at failure, the work hardening rate of the composites should also be modelled.

As mentioned above, thermal residual stresses also play an important role in the strengthening of the composite and should be included in the contributions to the yield strength because they are responsible for generating a high dislocation density in the matrix. Arsenault and Shi [10] proposed a model based on prismatic punching. The reinforcement is modelled as parallelepiped particles and punching occurs equally on all faces of the particles. The increase in yield strength is given by

$$\sigma_r = 2\alpha\mu\left(\frac{\boldsymbol{b} V_f \varepsilon}{1 - V_f}\right)^{1/2} R^{1/3}\left(1 + \frac{2}{R}\right)^{1/2}\left(\frac{1}{V}\right)^{1/6} \quad (6)$$

where ε is the misfit strain and is equal to $(\Delta\alpha\Delta T)/2$, R is the fibre aspect ratio and is equal to d/L, V is the volume of the fibre. $R < 1$ represents the whisker morphology as $R > 1$ represents the platelet morphology. For the present composites with $d = 0.5$ μm, $L = 7$ μm (L and d are the average length and diameter of the whiskers in the composite), $V = 1.4$ μm^3 and $\Delta T = 500$ °C, σ_r is equal to 80 MPa, which is quite significant. Therefore, when thermal dislocations are generated at the interface, σ_r should be added to σ_d to account fully for the contribution of the whiskers to the yield strength.

While it may be argued that many dislocations will be removed by normal recovery processes during cooling to room temperature after squeeze casting, it is very unlikely that many dislocations would be lost during refrigeration from room temperature to −196 °C. The refrigeration experiments, therefore, provide a useful evaluation of Arsenault and Shi's model by using it to predict the increase in yield strength after refrigeration. Using the values given above and $\Delta T = 200$ °C, $\sigma_r = 40$ MPa. This value compares excellently with the experimental values of 35–43 MPa.

The TEM observations showed that there are clear microstructural differences between the composites and, from the above discussion, the three different equations below can be proposed to predict the yield strength of the Al–Si, Mg and Cu binary alloy composites. The Al–Si specimens are characterized by a well developed subgrain structure. In this case, as the punching of the dislocations at the particle interface is not significant (dislocations rearranged to form subgrain boundaries), the dispersion strengthening term is a good approximation of the whisker strengthening effect. In the Al–Mg and Al–Cu specimens dislocations are punched around the whiskers and the prismatic model is used to predict the contribution of the whiskers. It is uncertain how σ_r should be added to the other terms (σ_{my} and σ_p). For simplicity, it was chosen to add the contributions as shown below.

$$\text{Al–Si:} \quad \sigma_{cy} = \sigma_{my} + \sigma_d + \sigma_g \quad (8)$$

$$\text{Al–Mg:} \quad \sigma_{cy} = \sigma_{my} + \sigma_r + \sigma_d \quad (9)$$

$$\text{Al–Cu:} \quad \sigma_{cy} = \sigma_{my}(F) + \sigma_p + \sigma_r + \sigma_d \quad (10)$$

The yield strengths of Al–Mg and Al–Cu in the T6 condition, for which ΔT and σ_p can be easily determined and of the Al–Si in F condition (in T6, precipitates appeared in the matrix which would have to be taken into account) were calculated. The calculated and experimental yield strengths are shown in Fig. 10. The difference between the experimental and calculated values is minimal (30 MPa) and could probably be accounted for by load transfer, which would then participate in the strengthening by 18% in Al–Si (F), 9% in Al–Mg (T6) and 4% in Al–Cu (T6). It is smaller for the age-hardened composite where the precipitates are believed to be the main source of strengthening.

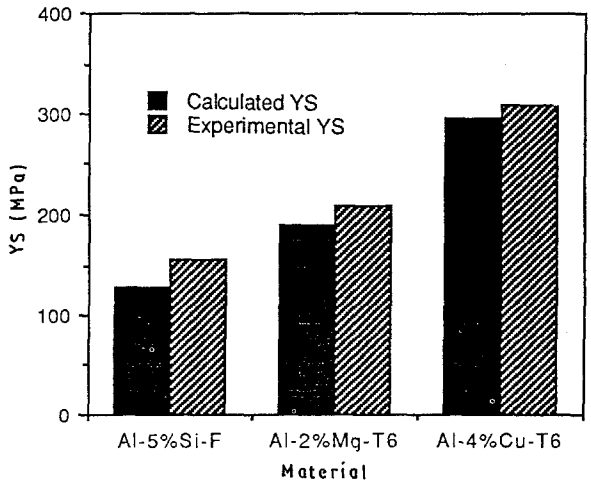

Figure 10 Calculated and experimental yield strengths of the Al–5%Si–F, Al–2%Mg–T6 and Al–4%Cu–T6 composites.

The agreement between theoretical and experimental values shows that this approach holds great promise for modelling the mechanical behaviour of whisker (and presumably also particulate) reinforced composites.

Finally, TEM observation of deformed specimens revealed characteristic deformation modes which depended on the matrix composition and microstructure. The fracture process in particulate MMCs has been well described by Humphreys [8] and similar failure mechanisms operate in the Al–Si, Al–Mg and Al–Cu whisker-reinforced composites. During deformation, dislocations accumulate at particles, causing an increase in local stress. Secondary dislocations are then generated as a result of local plastic relaxation. As straining continues, dislocation motion becomes more difficult next to the particles and the local stress rises. When it exceeds the stress necessary for decohesion or particle cracking, voids or cracks nucleate and failure occurs [17, 18]. Relaxation of stresses will be easier in the Al–Si matrix (subgrains form during relaxation of thermal stresses) than in the Al–Mg matrix, where solute hardening occurs. As magnesium segregates at the interface to form oxide, the interfacial layer and the depletion of solute atoms in the matrix weakens the interfacial regions, leading to the observed decohesion as local stresses rise. The matrix will be the hardest when age-hardening precipitates are present, resulting in more whisker cracking as plastic flow of the matrix is more difficult as observed in the Al–Cu and 6061 composites.

Thus the ease of plastic flow in the matrix and the presence of interfacial precipitates will determine whether failure occurs by ductile failure of the matrix (Al–Si) or decohesion (Al–Mg) or whisker cracking (Al–Cu). However, the macroscopic ductilities do not seem to depend solely on the microscopic failure mechanisms and are believed to be closely related to relatively gross microstructural features such as porosity, whisker clusters and inclusions.

5. Conclusions

The mechanical behaviour of different SiC_w/Al composites has been investigated. Their microstructures have been examined and the strengthening mechanisms occurring in each material were determined.

1. Three different types of composite matrices were distinguished and the yield strength of each was calculated using a micromechanical approach which gave reasonable agreement with the experimental values.

2. Alloying elements exert a strong influence on the strength of the composites. Their effects can be understood with reference to the microstructure induced.

3. The composites age more rapidly than the corresponding unreinforced alloy.

4. The mechanical properties of the Al–4%Cu composite are affected by cooling treatments as additional dislocations are generated.

5. Heat treatments can be used to generate different dislocation structures and precipitate sizes, which would then result in a defined and if possible predictable yield strength.

6. The ideal SiC_w/Al composite (high yield strength and good ductility) must have an age-hardenable matrix. It should be in a peak aged condition and a cooling step could be added to the heat-treatment schedules in order to increase its yield strength.

7. The whisker/matrix interface is strong and whether decohesion or particle cracking occurs during deformation depends on the matrix composition and microstructure.

Acknowledgement

The authors thank Honda R. and D. Co. Ltd, Japan, for financial support during the course of this work.

References

1. J. M. PAPAZIAN and P. N. ADLER, *Metall. Trans.* **21A** (1990) 401.
2. V. C. NARDONE and K. M. PREWO, *Scripta Metall.* **20** (1986) 43.
3. V. C. NARDONE, *ibid.* **21** (1987) 1313.
4. M. TAYA and R. J. ARSENAULT, *ibid.* **21** (1987) 349.
5. A. LEVY and J. M. PAPAZIAN, *Metall. Trans.* **21A** (1990) 411.
6. R. J. LEDERICH and S. M. L. SASTRY, *Mater. Sci. Engng* **55** (1982) 143.
7. D. L. McDANELS, *Metall. Trans.* **16A** (1985) 1105.
8. F. J. HUMPHREYS, in "Proceedings of the 9th Risø International Symposium on Metallurgy and Materials Science," edited by S. I. Anderson, H. Lilholt and O. B. Pedersen (1988) pp. 51–74.
9. R. J. ARSENAULT and M. TAYA, ICCM-5, edited by W. Harrigan, J. Strife and A. Dhingra (The Metallurgical Society of AIME, Warrendale, PA, 1988) pp. 21–36.
10. R. J. ARSENAULT and N. SHI, *Mater. Sci. Engng.* **81** (1986) 175.
11. B. DERBY and J. R. WALKER, *Scipta Metall.* **22** (1988) 529.
12. R. J. ARSENAULT and R. M. FISHER, *ibid.* **17** (1983) 67.
13. M. VOGELSANG, R. J. ARSENAULT and R. M. FISHER, *Metall. Trans.* **17A** (1986) 379.
14. R. J. McELNOY and Z. C. SKHOPIAK, *Int. Met. Rev.* **17** (1972) 175.
15. A. W. THOMPSON, *Metall. Trans.* **8A** (1977) 833.
16. A. J. E. FOREMAN and M. J. MAKIN, *Canad. J. Phys.* **45** (1967) 511.
17. S. H. GOODS and L. M. BROWN, *Acta Metall.* **27** (1979) 1.
18. J. D. EMBURY, *Metall. Trans.* **16A** (1985) 2191.

Received 5 September
and accepted 19 November 1990